A Finite Element Model of the Embryonic Zebrafish Heart Electrophysiology

https://doi.org/10.1016/j.cmpb.2022.107281

Ludovica Cestariolo[1], Giulia Luraghi[1], Pierre L'Eplattenier[2], Jose Felix Rodriguez Matas[1]

[1]Laboratory of Biological Structure Mechanics (LaBS), Department of Chemistry, Materials and Chemical Engineering "Giulio Natta", Politecnico di Milano, Milan, Italy

ludovica.cestariolo@polimi.it

giulia.luraghi@polimi.it

josefelix.rodriguezmatas@polimi.it

[2]Livermore Software Technology Corporation, CA, US

pierre.leplattenier@ansys.com

Address for correspondence:

Ludovica Cestariolo

Laboratory of Biological Structure Mechanics (LaBS), Dept. of Chemistry, Materials and Chemical Engineering "Giulio Natta", Politecnico di Milano

Piazza L. Da Vinci, 32, 20133 Milan, Italy

ludovica.cestariolo@polimi.it

+39 3407532656

Abstract

Background and objective: *In the last 30 years, a growing interest has involved the study of zebrafish thanks to its physiological characteristics similar to those of humans. The aim of the following work is to create an electrophysiological computational model of the zebrafish heart and lay the foundation for the development of an in-silico model of the zebrafish heart that will allow to study the correlation between pathologies and drug administration with the main electrophysiological parameters as the ECG signal.*

Methods: *The model considers a whole body and the two chambers of three days post fertilization (3 dpf) zebrafish. A four-variable phenomenological action potential model describes the action potential of different heart regions. Tissue conductivity was calibrated to reproduce the experimentally described activation sequence.*

Results: *The model is able to correctly reproduce the activation sequence and times found in literature, with activation of the atrium and ventricle that correspond to 36 and 59 ms, respectively, and a delay of 14 ms caused by the presence of the atrioventricular band (AV band). Moreover, the obtained in-silico ECG reflects the main characteristics of the zebrafish ECG in good agreement with experimental records, a P-wave with a duration of approximately the total atrial activation, followed by a QRS complex of approximately 109 ms corresponding to ventricle activation.*

Conclusions: *The model allows the assessment of the main electrophysiological parameters in terms of activation sequence and timing, reproducing monopolar and bipolar ECG signals in line with experimental data. Coupling the proposed model with an electrophysiological detailed action potential model of zebrafish will represent a significant breakthrough toward the development of an in-silico zebrafish heart.*

Keywords: Zebrafish, Computational Model, Electrophysiology, Action Potential, ECG

1. Introduction

In the last 30 years, a growing interest has involved the study of zebrafish thanks to characteristics that make this animal very attractive for different fields of study. First, zebrafish has small dimensions (~ 3 – 5 cm) and results in simple and economical maintenance compared to mammals. In addition, the zebrafish embryos are transparent until 30 days post fertilization (dpf), which is very useful for investigating heart development. After 24 hours post fertilization (hpf), the embryo has formed most of the organs, including a contracting heart tube and a nervous system, even though the latter is not yet fully innervated to the heart [1]. Differently from mammals, zebrafish is able to regenerate up to 20 % of the myocardium without scar formation [2]. Its high fertility (~ 200 eggs per week) is ideal for extensive statistical analysis [1] also considering that, in agreement with the European Commission Directive from 2010 (Directive 2010/63/EU), until 5 dpf, when the independent feeding starts, zebrafish is not yet subjected to the regulation for animal experimentation, representing in this way an alternative to animal experimentation [3].

The interest in zebrafish is also connected to electrophysiology. In fact, the physiology of zebrafish is very close to the human one, showing similar spontaneous heart rate, a heart rate dependent QT-interval [4], and similar action potential (AP) shape and duration [5]. Additionally, the zebrafish shows the presence of 69 % of orthologues of human genes and reciprocally 71.4 % of human genes have at least one zebrafish orthologue [6]. These percentages are found to be striking similar to other mammals (i.e., 82 % in mouse and rat or 79 % in dog [8]). Moreover, many genes encoding for ion channels in zebrafish have orthologues in human, leading to similarities in zebrafish and human cardiac electrophysiology [7]. Further, in relation to human cardiac disease and disease-related genes, the Online Mendelian In-heritance in Man (OMIM) database shows that 82 % of human genes have at least one zebrafish orthologue [9], and that 96 % of human dilated cardiomyopathy-associated genes have orthologues in zebrafish [10]. However, there are

important differences in ion channels underlying the cardiac action potential between zebrafish and humans that need to be kept in mind when using the zebrafish heart as a surrogate for pharmacological and pathophysiological studies of human cardiac electrophysiology [11]. For all these reasons, zebrafish has been proposed as a potential model for genetic and pharmacological screenings for all factors affecting heart functions.

Despite the rising interest, few studies developed a computational model of the zebrafish heart to date. A first study from *Qian et al.* [12] concerns the development of a three-dimensional discrete model for 48 and 72 hpf larval zebrafish ventricular fibers (LZVF) to assess the action potential propagation. The model used the phenomenological FitzHugh – Nagumo (FHN) equations to describe transmembrane currents, and then FHN parameters were adjusted using published AP and cell size data for the zebrafish embryos. The use of LZVF, has the benefit of reducing computational costs if compared to a complete 3D simulation of the heart. Still, at the same time, it does not give any information on the electric propagation on the entire heart, its conductance, and the activation pattern. A more comprehensive study was carried out by *Crowcombe et al.* [5], in which a 3D model of a 3 dpf larval zebrafish was used to simulate the heart electrical activity and investigate how the ECG signal is related to the heart structure and the position of the electrodes. Also in this work, FitzHugh – Nagumo equations adjusted were used. The main limitation of this work is the unphysiological stimulation which leads to an unphysiological propagation of the action potential in the heart and inaccurate ECG waveforms.

This work aims at developing an accurate finite element model of the 3 dpf zebrafish embryo heart electrophysiology to recreate physiological activation times and patterns and how they are modulated by the electric characteristics of the myocardial tissue to reproduce realistic *in-silico* monopolar and bipolar electrocardiograms. This model sets the basis for the development of an *in-silico* model of the zebrafish heart.

2. Material and Methods

2.1 Governing equations

The electric propagation in the heart and body of zebrafish was modeled using the bidomain model for the heart coupled with the equation of volume conductor for the body [13]. The bidomain model can be simplified to the well-known monodomain model in the case of tissue isotropy or equal anisotropy [13]. For the zebrafish, no evidence of tissue anisotropy or the presence of muscular fibers is reported in literature [14] allowing, therefore, the assumption of tissue isotropy when modeling its electrophysiology. In this case, the electrophysiology problem is solved in two steps. First, the propagation of the transmembrane potential is obtained by solving the monodomain model:

$$\boldsymbol{\nabla} \cdot (\mathbf{D}\boldsymbol{\nabla}\mathrm{V_m}) = \mathrm{C_m}\frac{\partial \mathrm{V_m}}{\partial \mathrm{t}} + \mathrm{J_{ion}}(\mathrm{V_m}, \mathbf{s}) \quad \text{in } H \tag{1}$$

$$\frac{\partial \mathbf{s}}{\partial \mathrm{t}} = \mathrm{f}(\mathbf{s}, \mathrm{V_m}, \mathrm{t}) \quad \text{in } H \tag{2}$$

$$\mathbf{n} \cdot (\mathbf{D}\boldsymbol{\nabla}\mathrm{V_m}) = 0 \quad \text{in } \partial H \tag{3}$$

where H represents the heart volume and ∂H its bounding surface with outer normal $\mathbf{n}$; $\mathrm{V_m}$ the transmembrane potential; $\mathrm{C_m}$ the specific membrane capacitance (assumed $1\ \mu\mathrm{F/cm^2}$); $\mathbf{D}$ the isotropic effective conductivity tensor of the myocardium defined in terms of the intracellular conductivity tensor, $\mathbf{D_i} = \sigma_\mathrm{i}\mathbf{I}$ (σ_i the intracellular conductance and $\mathbf{I}$ the identity matrix), as $\mathbf{D} = \lambda/(1+\lambda)\,\sigma_\mathrm{i}\mathbf{I}$, with λ the intracellular to extracellular conductivity ratio (assumed, as in previous studies [5][12], to be 1); and $\mathrm{J_{ion}}(\mathrm{V_m}, \mathbf{s})$ the transmembrane ionic current, with $\mathbf{s}$ the vector of state variables associated with the ionic model.

With the transmembrane potential in the heart at hand, the extracellular potential in the heart, $\mathrm{V_e}$, and body, $\mathrm{V_B}$ (necessary to extract the ECG signal at the body surface) are obtained by solving the following set of partial differential equations:

$$(1+\lambda)\boldsymbol{\nabla} \cdot (\mathbf{D}\boldsymbol{\nabla}\mathrm{V_e}) = -\boldsymbol{\nabla} \cdot (\mathbf{D}\boldsymbol{\nabla}\mathrm{V_m}) \quad \text{in } H \tag{4}$$

$$\boldsymbol{\nabla} \cdot (\mathbf{D}_B\boldsymbol{\nabla}\mathrm{V}_B) = 0 \quad \text{in } B \tag{5}$$

$$\mathbf{n} \cdot \big((1+\lambda)(\mathbf{D}\boldsymbol{\nabla}\mathrm{V}_e)\big) = \mathbf{n} \cdot (\mathbf{D}_B\boldsymbol{\nabla}\mathrm{V}_B) \quad \text{in } \partial H \tag{6}$$

$$\mathbf{n}_B \cdot (\mathbf{D}_B \nabla \mathrm{V}_B) = 0 \qquad \text{in } \partial B \tag{7}$$

$$\mathrm{V}_B = \mathrm{V}_e \qquad \text{in } \partial H \tag{8}$$

where B represents the body volume (not including the heart) and ∂B its bounding outer surface with outer normal $\mathbf{n}_B$, and $\mathbf{D}_B = \sigma_B \mathbf{I}$ the isotropic extracellular conductivity tensor of the body.

In summary, the governing equations comprise a parabolic reaction-diffusion equation coupled with a set of ordinary differential equations, representing the ionic currents through the cellular membrane, that define the propagation of the transmembrane potential in the heart (Equations 1-3), together with two coupled elliptic partial differential equations describing the extracellular potential in the heart (Equation 4) and the body of zebrafish (Equation 5) modeled as a passive volume conductor.

2.2 Action potential model

The four-variables minimal model (BV4) proposed by *Bueno-Orovio et al.* [15] was used in this study to reproduce the action potential of the different parts of the model. The BV4 is a phenomenological model that uses only four state variables to reproduce many AP shapes while accurately reproducing the AP duration (APD) and conduction velocity restitution curves.

The action potential model is defined as follows:

$$\frac{\partial \mathrm{V_m}}{\partial \mathrm{t}} = -(\mathrm{J_{fi}} + \mathrm{J_{so}} + \mathrm{J_{si}}) \tag{9}$$

$$\frac{\partial \mathrm{v}}{\partial \mathrm{t}} = 1 - \mathrm{H}(\mathrm{V_m} - \theta_\mathrm{v}) - \frac{1}{\tau_\mathrm{v}^-}(\mathrm{v}_\infty - \mathrm{v}) - \frac{\mathrm{v}}{\tau_\mathrm{v}^+}\mathrm{H}(\mathrm{V_m} - \theta_\mathrm{v}) \tag{10}$$

$$\frac{\partial \mathrm{w}}{\partial \mathrm{t}} = 1 - \mathrm{H}(\mathrm{V_m} - \theta_\mathrm{w}) - \frac{1}{\tau_\mathrm{w}^-}(\mathrm{w}_\infty - \mathrm{w}) - \frac{\mathrm{w}}{\tau_\mathrm{w}^+}\mathrm{H}(\mathrm{V_m} - \theta_\mathrm{w}) \tag{11}$$

$$\frac{\partial \mathrm{s}}{\partial \mathrm{t}} = \frac{1}{2}\left[1 + \tanh\left(\mathrm{k_s}(\mathrm{V_m} - \mathrm{u_s})\right)\right] - \frac{\mathrm{s}}{\tau_\mathrm{s}} \tag{12}$$

where $\mathrm{H}(\cdot)$ is the standard Heaviside function, and the three currents per unit surface $\mathrm{J_{fi}}$, the fast inward current, $\mathrm{J_{so}}$ the slow outward current, and $\mathrm{J_{si}}$ the slow inward current are:

$$J_{fi} = -\frac{1}{\tau_{fi}} v \cdot (V_m - \theta_v) H(V_m - \theta_v) H(u_u - V_m) \quad (13)$$

$$J_{so} = \frac{1}{\tau_o}(V_m - u_o)[1 - H(V_m - \theta_w)] + \frac{1}{\tau_{so}} H(V_m - \theta_w) \quad (14)$$

$$J_{si} = -\frac{1}{\tau_{si}} w \cdot s \cdot H(V_m - \theta_w) \quad (15)$$

with τ_v^-, τ_w^-, τ_{so}, τ_s, τ_o the time constants:

$$\tau_v^- = 1 - \tau_{v1}^- H(u - \theta_v^-) + \tau_{v2}^- H(u - \theta_v^-) \quad (16)$$

$$\tau_w^- = \tau_{w1}^- + \frac{1}{2}(\tau_{w2}^- - \tau_{w1}^-)\left[1 + \tanh\left(k_w^-(u - u_w^-)\right)\right] \quad (17)$$

$$\tau_{so} = \tau_{so1} + \frac{1}{2}(\tau_{so2} - \tau_{so1})\left[1 + \tanh\left(k_{so}(u - u_{so})\right)\right] \quad (18)$$

$$\tau_s = [1 - H(u - \theta_w)]\tau_{s1} + \tau_{s2} H(u - \theta_w) \quad (19)$$

$$\tau_o = [1 - H(u - \theta_o)]\tau_{o1} + \tau_{o2} H(u - \theta_o) \quad (20)$$

The parameters of the BV4 model were obtained by fitting the numerical AP model to the experimental recording of the zebrafish action potential in different heart regions [16][17] by means of non-linear regression analysis (R^2 over 0.98), as shown in Figure 1. The model parameters for the atrium and ventricle myocytes are found in Table S.1 in the supplemented materials.

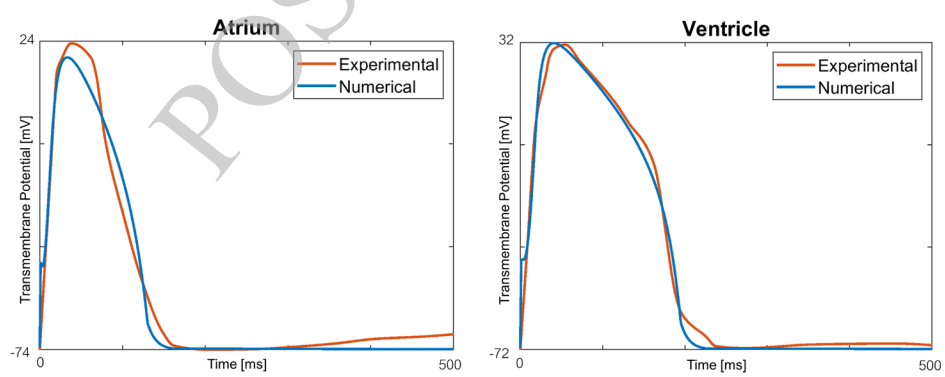

Figure 1. Fitting of the BV4 numerical curves to the experimental recording of the zebrafish AP for atrium (left) and ventricle (right). The fitting was obtained by simulating an isolated cell. Experimental data from [16].

2.3 Model geometry

Compared to the human heart, the zebrafish heart has a very simple structure: it is composed of two chambers (one atrium and one ventricle) and at 3 dpf has a size of approximately 70 µm evaluated from sinoatrial region to the ventricular base [5]. The model (Figure 2) is based on the geometry from *Crowcombe et al.* [5]. It consists of three parts: the body, the heart chambers, and the heart myocardium. The body has a surface of 280 μm^2 with a total volume of 9.62 μm^3, while the heart, which is positioned close to the ventral surface, has a surface area of 7.1 μm^2 with an average wall thickness of ~ 2.5 µm. The heart orientation is obtained by aligning the segment that runs from the tip of the sinous venosus to the one of the ventricles with the longitudinal axis of the body.

The heart myocardium is composed of four main regions: the sinoatrial region (SAR), which is the area where the stimulus starts, the atrial wall, the atrio-ventricular band (AV band), and the ventricular wall (right panel in Figure 2).

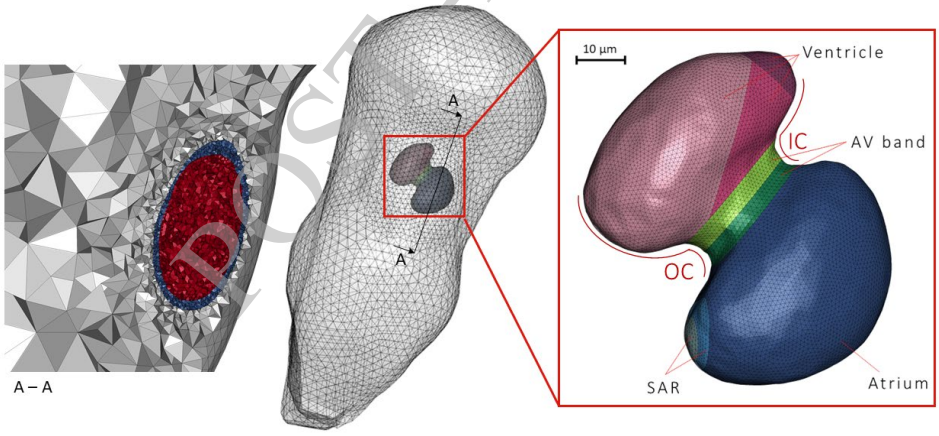

Figure 2. Ventral view (head on the top and tail on the bottom) of the complete geometry of the 3 dpf zebrafish model (middle panel) detailing the different parts of the heart model (right panel) and an internal section of the heart (left panel) showing the ventricular wall (blue) and the ventricular cavity (red). OC and IC in the right panel indicate the outer curvature and the inner curvature of the ventricle wall respectively.

The SAR, AV band, and ventricle were further divided, as shown in Figure 3, to account for differences in conduction velocity, leading to different activation times, reported in literature [14][18]. In particular, the sinoatrial region comprises two parts: SAR1 and

SAR2. This allows the recreation of the experimentally observed ring-like activation of the pacemaker cells [18]. The AV band is composed of two rings, one on the atrium side and one on the ventricle side, named AVband1 and AVband2, respectively. For these two parts, different action potential models were assigned. Specifically, the action potential model of the atrium was imposed to the AVband1 and the one of the ventricle to the AVband2. Lastly, the ventricular wall was divided into three regions (Figure 3) called Ventricle1, Ventricle2, and Ventricle3 associated with the apex-to-base conduction heterogeneity reported in literature [14].

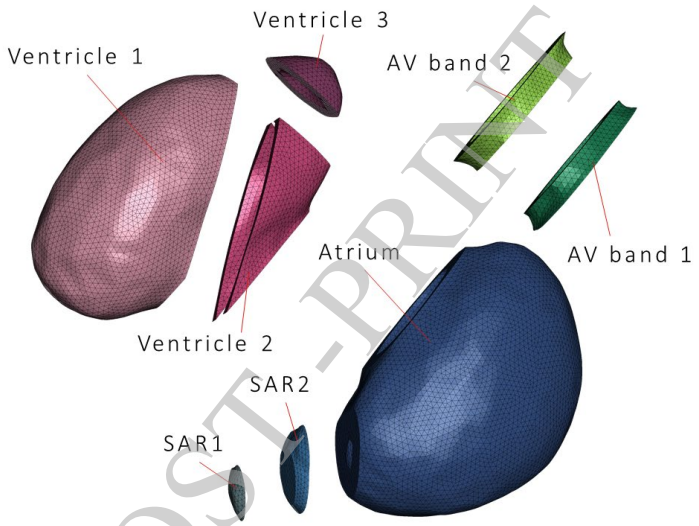

Figure 3. Sub-parts of the atrium, AV band, and ventricle used to recreate the experimental features.

The geometry was then discretized with tetrahedral elements with an element size of ~ 0.6 µm on average for the heart to obtained at least three elements in the wall thickness. A sensitivity analysis was performed to ensure that results were mesh element size independent. Figure S1 in the supplemented material shows the result of the analysis. For the body, instead, the mesh was generated by imposing a growth factor of 1.4 moving away from the heart region and resulting in an element size average value of ~ 5.6 µm. The model comprises 546142 elements and 94860 nodes, with 247309 elements and 53415 nodes in the heart.

2.4 Calibration of myocardial conductivity values

Evidence of anisotropy and the existence of muscle fibers in the zebrafish heart tissue was not found in literature, but was found the evidence of heterogeneity in electric propagation [14]. In this regard, it has been reported that the cardiomyocytes that form the myocardial outer curvature (OC), which becomes the ventricular apex, conduct the signal about three times faster than those that characterize the inner curvature (IC), which develops into the ventricular base [14] (see Figure 2). Based on this evidence, the heart tissue was modeled as isotropic with different conductivity values associated with different heart regions. Hence, the tissue conductivities assigned to the different parts shown in Figure 3 were calibrated such that the conduction velocities in the three different parts of the ventricle reported in [14] were reproduced by the model. Since the conduction velocity in the atrium is not reported in [14], but the total activation time instead, for this region, the value of the conductance was set to match the total activation time reported in [14]. On the other hand, the body conductivity has been set to reproduce the correct ECG signal amplitude [18]. Table 1 shows the results of the calibration process.

Table 1. Tissue intracellular and extracellular conductivities used in the model

Part	Intracellular conductivity (mS)	Extracellular conductivity (mS)
SAR1	2.89e-06	2.89e-06
SAR2	8.67e-06	8.67e-06
Atrium	2.60e-05	2.60e-05
AVband1	2.00e-07	2.00e-07
AVband2	3.00e-07	3.00e-07
Ventricle1	3.00e-06	3.00e-06
Ventricle2	3.00e-07	3.00e-07
Ventricle3	9.00e-08	9.00e-08
Body	-	1.60e-04

2.5 Stimulation and numerical simulation

The model was stimulated at the SAR with a basic cycle length (BCL) of 500 ms corresponding to a heart frequency of 2 Hz, close to the spontaneous heart rhythm of zebrafish [5]. The action potential model was implemented as a Usermaterial within the

multiphysics finite element solver LS-DYNA (ANSYS, Canonsburg, PA, USA) used to solve the complete set of equations of the governing equations with a fixed time step of 0.02 ms.

3. Results

3.1. Action potential

Figure 4 shows the numerical APs obtained for the atrium and ventricle in the 3D model.

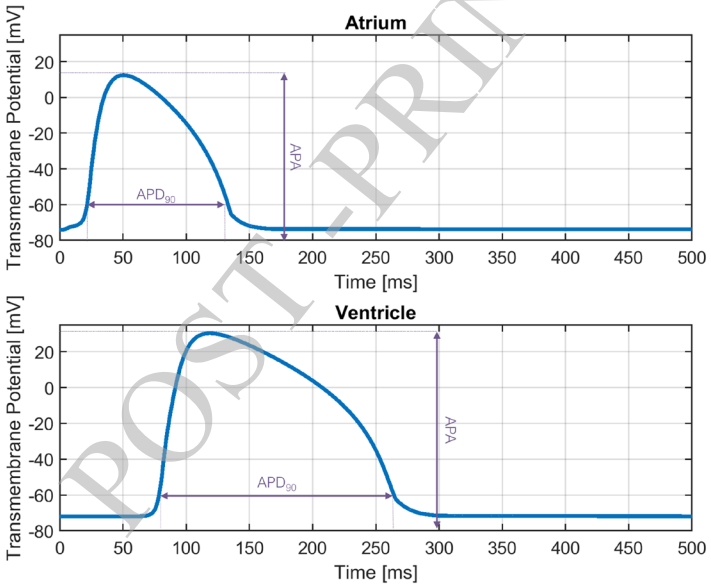

Figure 4. Experimental [16] *and numerical action potential for atrium (top) and ventricle (bottom).*

The main characteristics of the action potential morphology (i.e., APD_{90}, AP amplitude (APA), maximum, and minimum AP derivatives) were assessed and compared with experimental values reported in literature [5][12][17]. This comparison is reported in Table 2. In general, the morphology of the AP obtained in the 3D simulations is in good agreement with experimental values. Only the APD_{90} in the ventricle is slightly underestimated with respect to the experimental range. This may be explained because the calibration of the AP model was performed using isolated cell recordings which may differ

from measurements performed at tissue level by means of microelctrodes.

*Table 2. Comparison of AP morphology between model and experiments from literature. * Only experimental value available in literature.*

	AP marker	Model	Experiment [5][12][17]
Atrium	APD_{90} (ms)	118.64	102 ÷ 174.48
	APA (mV)	91.95	80.1 ÷ 110.65
	Max der. (V/s)	8.80	7.5 ÷ 9
	Min der. (V/s)	-2.28	-3.99*
Ventricle	APD_{90} (ms)	183.90	215.88 ÷ 328,12
	APA (mV)	102.26	89.03 ÷ 117.97
	Max der. (V/s)	6.38	2.26 ÷ 8.74
	Min der. (V/s)	-1.95	-1.69*

3.2. Activation times and sequence

The total activation time of the heart predicted by the model was 134 ms which compares well with the 125 ms reported in the experiments [14]. The electric signal took 36 ms to activate the atrium, starting from the SAR region where the stimulus is applied, followed by a 25 ms delay in the AV band to then propagate to the ventricles where the signal propagates following the outer curvature of the ventricle toward the arterial pole (Figure 5D) to fully depolarize the ventricle in 73 ms. These partial results are in good agreement with the experimental data reported in [14], for which the atrium depolarizes in 35 ms, with a delay of the order of 25 ms in the AV band, and 75 ms for the depolarization of the ventricle. Table 3 summarizes the experimental and *in-silico* results.

Table 3. Comparison of activation times between model and experiments from literature.

	Model	Experimental [14]
Atrium	36 ms	35 ms
AV band	25 ms	25 ms
Ventricle	73 ms	75 ms

For what concerns the activation sequence, Figure 5 shows how the activation starts from the SAR, where the pacemaker cells are located (Figure 5A). The activation then

continues towards the entire atrium (Figure 5B), the AV band (Figure 5C), and finally, the signal propagates into the ventricle following the characteristic apex-to-base pattern (Figure 5D and Figure 5E). The same sequence is followed during the repolarization of the atrium and ventricle, i.e., the first tissue to depolarize is also the first tissue to repolarize, as shown in Figure 5D to Figure 5H. The obtained results of the activation and repolarization sequence were found to be in line with optical mapping performed on a 3 dpf zebrafish heart [14] (see Figure 1a and Supplementary Movie 2 in [14]).

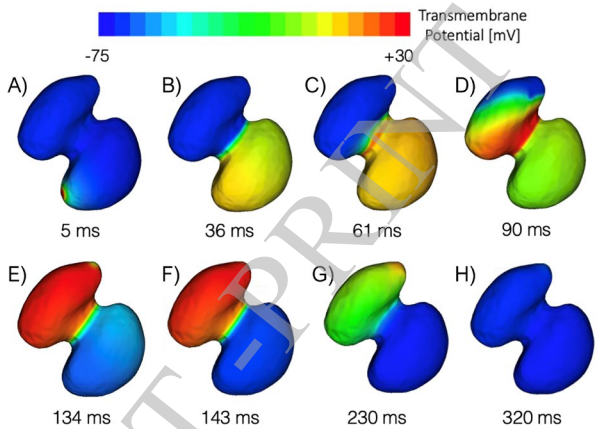

Figure 5. Significant frames of the activation sequence of the 3 dpf zebrafish heart model.

3.3. ECG

In this work, both monopolar and bipolar ECGs were assessed and compared with experimentally registered ECG signals.

Firstly, monopolar ECGs (Figure 6) for the atrio-ventricular and ventricular region were extracted by selecting specific nodes on the body surface, shown in Figure 6A, allowing the comparison with the *in vivo* signals reported in the study of *Crowcombe et al.* [5] for a 3 dpf zebrafish.

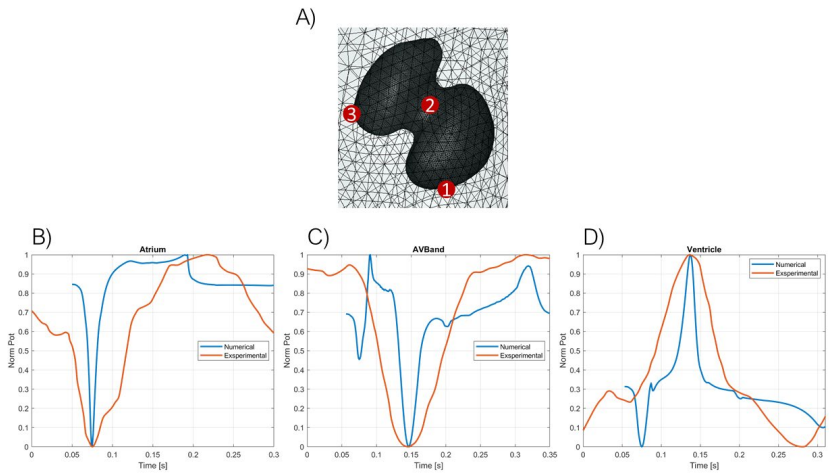

Figure 6. Monopolar ECGs: A) Considered body surface nodes for the ECG analysis (1: atrial, 2: middle, 3: ventricular), B) C) D) comparison between experimental [5] and in-silico signals.

Besides the differences with the experimental records, the simulated monopolar waveforms show the same polarity and characteristics of the experimental waveforms, indicating the correct activation sequence captured by the model and described in the previous paragraph. The most significant differences are associated with the duration of the QRS complex (lower in the simulation) and the amplitude of the P-wave (higher in the simulation) (see Figure 6C and Figure 6D). For node 2, selected in the middle region (i.e., AV band), both the model and recording showed a biphasic behavior of the P wave and a positive T wave (Figure 6C). Similarly, in the monopolar ECG computed on node 3, in the ventricular region, the results from the simulation are in line with experimental recordings showing a negative P-wave followed by a positive QRS complex and a negative T-wave (Figure 6D).

A bipolar ECG was also computed between the two electrodes shown in Figure 7 that were located on the body surface in correspondence of the ventricular base (electrode +) and ventricular apex (electrode -). The *in-silico* ECG (Figure 7) is found to be in good agreement with *in vivo* recorded zebrafish ECG [19] [20]. Namely, the P wave showed a duration of 43 ms, in line with the total atrial activation (36 ms). The relatively high amplitude of the P wave is due to the size of the atrium that, at 3 dpf, has a size comparable

to that of the ventricle. It is worth noting that, even if in the adult zebrafish the P wave has an amplitude that is smaller than the one of the QRS complex, it still shows a higher amplitude than in human ECG [19]. The P wave is followed by the QRS complex, which shows a duration of 109 ms, comparable with the 111 ms obtained from experiments. Finally, the T wave showed a duration of 62 ms, in line with the experimental value of 54 ms. Moreover, the negative polarity of the T wave is consistent with the depolarization-repolarization pattern obtained *in-silico* and reported in experiments with 3 dpf embryos.

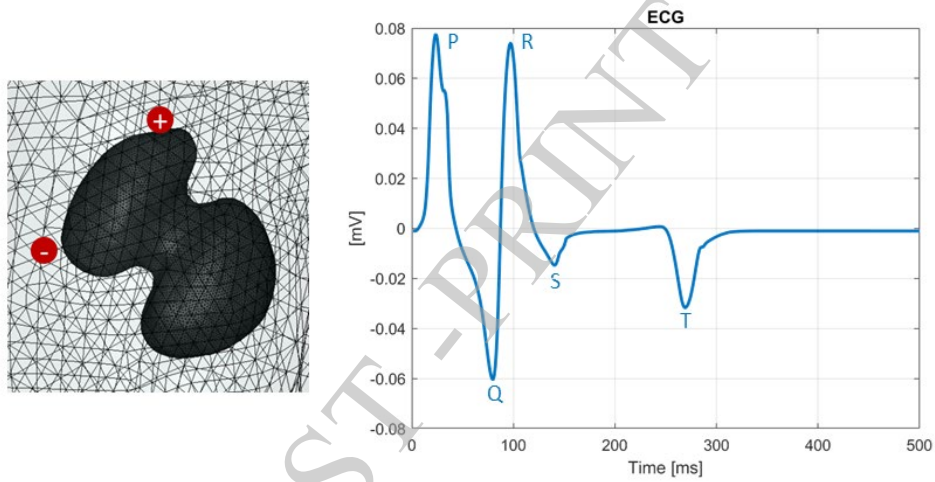

Figure 7. Body surface location of the electrodes for the bipolar ECG and the corresponding ECG trace. The positive electrode (+) is in correspondence of the ventricular base and the negative electrode (-) in correspondence of the ventricular apex.

The ECG parameters are summarized in Table 4.

Table 4. Bipolar ECG: comparison of the main ECG parameters between the model and the experimental recordings from literature

ECG parameters	Model	Experimental [20]
P width	43	36
QRS width (ms)	109	111
T width (ms)	62	54

4. Discussion

Despite the rising interest in zebrafish in the last decades, few studies have been

devoted to the development of a computational model of the zebrafish heart. This work develops a finite element model of the 3 dpf embryo electrophysiology accounting for different physiological characteristics described in literature. The decision to use a zebrafish embryo instead of an adult one was because it corresponds to one of the most popular zebrafish models. This popularity is related to the fact that embryos until 5 dpf represent a valid alternative to animal testing, that allows obtaining a significant amount of experimental data for model verification.

The model considers the cardiac tissue as isotropic since no evidence of tissue anisotropy or the presence of muscular fibers has been reported for the zebrafish cardiac tissue but considers the heterogeneity in conduction velocity in different areas of the heart [14]. In this regard, our numerical results indicate that considering conductivity heterogeneity in the ventricular tissue, as demonstrated by experiments, is required to describe the correct activation sequence of the zebrafish heart. On the other hand, considering homogeneous values (i.e., the conductivities of the outer and inner curvature are the same) results in a non-physiological activation sequence, with the apex of the heart being one of the last to be depolarized (results not shown). The proper activation sequence allows obtaining simulated monopolar ECGs in good agreement with experimental measurements from literature [5] [20] and a bipolar ECG that well reflects the main phases of activation and repolarization.

The main differences observed between the simulated ECG and the experimental records, in particular the duration of the QRS complex and the amplitude of the P-wave, are mostly associated to morphological differences that can be present between the simulated and the *in vivo* hearts. These differences are related to the high variability of experimental data for the zebrafish due to the high velocity in which the embryo and its heart develop. In this regard, a wider QRS complex indicates a larger size/volume ventricle for the *in vivo* measurements in comparison to the model. Increasing the ventricle size in the *in silico* model will not only make the QRS complex wider, but also reduce the amplitude of the P-wave relative to that of the QRS complex while increasing the

amplitude of the T-wave. Differences between simulation and experiments could also be associated with a difference in the thickness between the atrial (thinner) and ventricular (thicker) walls, which is not reported in the model but is found in literature [18][19].

This model is not exempt from limitations. One of the main limitations concerns the geometry of the 3 dpf embryo. The choice of the 3 dpf embryo is linked to the difficulty of finding images that allow the realization of a more advanced embryonal stage. The main difference between the embryo and the adult fish lies in the volume of the atrium compared to the ventricular one. This will result in a smaller amplitude on the P wave compared to the QRS one. Moreover, another difference is related to the repolarization sequence in the ventricle. In fact, looking at the experimental depolarization-repolarization sequence in the ventricle of a 3 dpf embryo, it is possible to see that they follow the same apex-to-base pattern resulting in a negative T wave. On the other hand, looking at adult recording ECGs, the T wave seems to be positive, suggesting that the repolarization occurs base-to-apex (as in humans). For this reason, future developments will mainly focus on modeling different geometries to account for different developmental stages of the embryos (i.e., 4 and 5 dpf). In fact, at these advanced stages, the heart rhythm is more stable, and the size of the atrium is significantly smaller than the ventricular one, being closer to those of the adult fish. This leads to *in-silico* ECG signals more similar to human ones. In addition, the model considers a constant wall thickness model for the atrium and ventricle. Future models should consider the actual thickness of the ventricle (considerably thicker than the atrium). This will contribute to achieving more realistic ECG signals, in particular the QRS complex.

Another fundamental aspect to consider in future developments is coupling the proposed model to an electrophysiological detailed AP model for zebrafish to assess the effect of the different ionic channels. Our group is working on its development which first version has already been published [21]. The use of the detailed AP model in the 3D simulation will allow the study of different cardiac pathologies and ionic channel mutations, as well as the effect that different drugs have on the electrophysiology of

zebrafish and how it is reflected at the ECG level. This work comprises the first step towards the development of an *in-silico* zebrafish heart.

Conflict of interest statement

Pierre L'Eplattenier reports a financial relationship with Livermore Software Technology Corporation outside the submitted work.

Credit authorship contribution statement

Ludovica Cestariolo: Conceptualization, Methodology, Investigation, Formal analysis, Writing – original draft, Writing – review & editing. **Giulia Luraghi:** Methodology, Writing – review & editing. **Pierre L'Eplattenier:** Methodology, Software, Writing – review & editing. **Jose F Rodriguez Matas:** Project administration, Conceptualization, Methodology, Interpretation of Results, Writing – review & editing.

Acknowledgments

Ludovica Cestariolo, Giulia Luraghi, and Jose F Rodriguez Matas are supported by a grant by the Italian Ministry of Education, University and Research (Grant number 1613 FISR2019_03221, CECOMES).

References

[1] K. L. Poon and T. Brand, "The zebrafish model system in cardiovascular research: A tiny fish with mighty prospects," *Glob. Cardiol. Sci. Pract.*, vol. 2013, no. 1, p. 9, Mar. 2013, doi: 10.5339/GCSP.2013.4.

[2] P. Nemtsas, E. Wettwer, T. Christ, G. Weidinger, and U. Ravens, "Adult zebrafish heart as a model for human heart? An electrophysiological study," *J. Mol. Cell. Cardiol.*, vol. 48, no. 1, pp. 161–171, Jan. 2010, doi: 10.1016/J.YJMCC.2009.08.034.

416 [3] S. Cassar, I. Adatto, J. L. Freeman, J. T. Gamse, I. Iturria, C. Lawrence, A.
417 Muriana, R. T. Peterson, S. Van Cruchten, and L. I. Zon, "Use of Zebrafish in
418 Drug Discovery Toxicology," *Chem. Res. Toxicol.*, vol. 33, no. 1, pp. 95–118, Jan.
419 2020, doi: 10.1021/acs.chemrestox.9b00335.
420 [4] M. Vornanen and M. Hassinen, "Zebrafish heart as a model for human cardiac
421 electrophysiology," *Channels*, vol. 10, no. 2, pp. 101–110, Jan. 2016, doi:
422 10.1080/19336950.2015.1121335.
423 [5] J. Crowcombe, S. S. Dhillon, R. M. Hurst, S. Egginton, F. Müller, A. Sík, and E.
424 Tarte, "3D Finite Element Electrical Model of Larval Zebrafish ECG Signals,"
425 *PLoS One*, vol. 11, no. 11, p. e0165655, Nov. 2016, doi:
426 10.1371/JOURNAL.PONE.0165655.
427 [6] K. Howe, M. D. Clark, C. F. Torroja, J. Torrance, C. Berthelot, M. Muffato, J. E.
428 Collins, S. Humphray, K. McLaren, L. Matthews, *et al.*, "The zebrafish reference
429 genome sequence and its relationship to the human genome," *Nature*, vol. 496,
430 no. 7446, p. 498, Apr. 2013, doi: 10.1038/NATURE12111.
431 [7] U. Ravens, "Ionic basis of cardiac electrophysiology in zebrafish compared to
432 human hearts," *Prog. Biophys. Mol. Biol.*, vol. 138, pp. 38–44, Oct. 2018, doi:
433 10.1016/J.PBIOMOLBIO.2018.06.008.
434 [8] A. Matsuya, R. Sakate, Y. Kawahara, K. O. Koyanagi, Y. Sato, Y. Fujii, C.
435 Yamasaki, T. Habara, H. Nakaoka, F. Todokoro, *et al.*, "Evola: Ortholog database
436 of all human genes in H-InvDB with manual curation of phylogenetic trees,"
437 *Nucleic Acids Res.*, vol. 36, no. suppl_1, pp. D787–D792, Jan. 2008, doi:
438 10.1093/NAR/GKM878.
439 [9] A. Asnani and R. T. Peterson, "The zebrafish as a tool to identify novel therapies
440 for human cardiovascular disease," *Dis. Model. Mech.*, vol. 7, no. 7, pp. 763–767,
441 2014, doi: 10.1242/DMM.016170.
442 [10] Y. H. Shih, Y. Zhang, Y. Ding, C. A. Ross, H. Li, T. M. Olson, and X. Xu,
443 "Cardiac transcriptome and dilated cardiomyopathy genes in zebrafish," *Circ.*

Cardiovasc. Genet., vol. 8, no. 2, pp. 261–269, Apr. 2015, doi: 10.1161/CIRCGENETICS.114.000702.

[11] M. Hassinen, J. Haverinen, M. E. Hardy, H. A. Shiels, and M. Vornanen, "Inward rectifier potassium current (I K1) and Kir2 composition of the zebrafish (Danio rerio) heart," *Pflugers Arch.*, vol. 467, no. 12, pp. 2437–2446, Dec. 2015, doi: 10.1007/S00424-015-1710-8.

[12] S. Qian and E. Tarte, "Finite element modelling of discontinuous action potential propagation in larval zebrafish and human cardiac tissue," *Phys. Biol.*, vol. 17, no. 1, 2019, doi: 10.1088/1478-3975/AB4D62.

[13] D. B. Geselowitz and W. T. Miller III, "A BIDOMAIN MODEL FOR ANISOTROPIC CARDIAC MUSCLE," *Ann. ofBiomedicalEngineering*, vol. 11, pp. 191–206, 1983, doi: 10.1007/BF02363286.

[14] D. Panáková, A. A. Werdich, and C. A. MacRae, "Wnt11 patterns a myocardial electrical gradient through regulation of the L-type Ca2+ channel," *Nat. 2010 4667308*, vol. 466, no. 7308, pp. 874–878, Jul. 2010, doi: 10.1038/nature09249.

[15] A. Bueno-Orovio, E. M. Cherry, and F. H. Fenton, "Minimal model for human ventricular action potentials in tissue," *J. Theor. Biol.*, vol. 253, no. 3, pp. 544–560, Aug. 2008, doi: 10.1016/J.JTBI.2008.03.029.

[16] A. A. Werdich, A. Brzezinski, D. Jeyaraj, M. Khaled Sabeh, E. Ficker, X. Wan, B. M. McDermott, C. A. MacRae, and D. S. Rosenbaum, "The zebrafish as a novel animal model to study the molecular mechanisms of mechano-electrical feedback in the heart," *Prog. Biophys. Mol. Biol.*, vol. 110, no. 2–3, pp. 154–165, Oct. 2012, doi: 10.1016/J.PBIOMOLBIO.2012.07.006.

[17] R. Arnaout, T. Ferrer, J. Huisken, K. Spitzer, D. Y. R. Stainier, M. Tristani-Firouzi, and N. C. Chi, "Zebrafish model for human long QT syndrome," *Proc. Natl. Acad. Sci. U. S. A.*, vol. 104, no. 27, pp. 11316–11321, Jul. 2007, doi: 10.1073/pnas.0702724104.

[18] M. Weber, N. Scherf, A. M. Meyer, D. Panáková, P. Kohl, and J. Huisken, "Cell-

accurate optical mapping across the entire developing heart," *Elife*, vol. 6, Dec. 2017, doi: 10.7554/ELIFE.28307.

[19] Y. Zhao, N. A. James, A. R. Beshay, E. E. Chang, A. Lin, F. Bashar, A. Wassily, and B. Nguyen, "Adult zebrafish ventricular electrical gradients as tissue mechanisms of ECG patterns under baseline vs. oxidative stress," *Cardiovasc. Res.*, vol. 117, no. 8, p. 1891, Jul. 2021, doi: 10.1093/CVR/CVAA238.

[20] E. Rendon-Morales, R. J. Prance, H. Prance, and R. Aviles-Espinosa, "Non-invasive electrocardiogram detection of in vivo zebrafish embryos using electric potential sensors," *Appl. Phys. Lett.*, vol. 107, no. 19, p. 193701, Nov. 2015, doi: 10.1063/1.4935249.

[21] L. Cestariolo, M. Bataller Martinez, J. M. Ferrero, and J. F. Rodriguez Matas, "A model for zebrafish ventricular action potential," Computing in Cardiology 2022.

Supplementary Material 1

Table S.1 summarizes the model parameters for the 4 variable model from Bueno Orovio et al. [12]. Parameters were identified by means of a non-linear regression analysis of action potential registries for atrium and ventricle reported in [13-14].

Table S.1. Parameters of the 2-variable model for Atrium and Ventricle myocytes

Parameter	Atrium	Ventricle
u_o	0.0000e+00	0.0000e+00
u_u	1.5500e+00	1.5500e+00
θ_v	3.0000e-01	3.0000e-01
θ_w	1.3000e-01	1.3000e-01
θ_v^-	6.0000e-03	6.0000e-03
θ_o	6.0000e-03	6.0000e-03
τ_{v1}^-	6.0000e+01	6.0000e+01
τ_{v2}^-	1.150e+03	1.1500e+03
τ_v^+	2.9197e+00	2.9197e+00
τ_{w1}^-	8.2093e+01	8.1986e+01
τ_{w2}^-	1.6369e+01	1.6369e+01
k_w^-	6.3673e+01	6.3914e+01
u_w^-	3.7379e-02	2.8531e-02
τ_w^+	1.0004e+02	1.7089e+02
τ_{fi}	9.9352e-01	9.9352e-01
τ_{o1}	4.3219e+02	4.3160e+02
τ_{o2}	9.9884e+00	9.9969e+00
τ_{so1}	1.0000e+01	1.0023e+01
τ_{so2}	1.8239e-01	1.8239e-01
k_{so}	1.0001e+00	1.1059e+00
u_{so}	6.1633e-01	7.3470e-01
τ_{s1}	9.9367e+00	7.0310e+00
τ_{s2}	8.1343e+00	9.1176e+00
k_s	1.0007e+00	1.0006e+00
u_s	6.6648e-01	8.4811e-01
τ_{si}	1.0004e+00	1.0005e+00
$\tau_{w\infty}$	2.5323e-01	2.5239e-01
w_∞^*	9.5335e-01	9.7163e-01

Supplementary Material 2

Figure S.1. Sensitivity mesh size analysis for the different parts of the zebrafish heart. The red column indicates the mesh size used in the simulations. Results confirm the

mesh independency of the conduction velocity